Comparative oxidation behavior of Nd-Fe-B magnets for potential recycling methods:

Onal, Mehmet Ali; Jönsson, Christian; Zhou, Wei; Van Gerven, Tom; Guo, Muxing; Walton, Allan; Blanpain, Bart

DOI:
10.1016/j.jallcom.2017.09.046

Document Version
Peer reviewed version

Citation for published version (Harvard):
Onal, MA, Jönsson, C, Zhou, W, Van Gerven, T, Guo, M, Walton, A & Blanpain, B 2017, 'Comparative oxidation behavior of Nd-Fe-B magnets for potential recycling methods: Effect of hydrogenation pre-treatment and magnet composition', *Journal of Alloys and Compounds*, vol. 728, pp. 727-738.
https://doi.org/10.1016/j.jallcom.2017.09.046

Accepted Manuscript

Comparative oxidation behavior of Nd-Fe-B magnets for potential recycling methods: Effect of hydrogenation pre-treatment and magnet composition

Mehmet Ali Recai Önal, Christian Jönsson, Wei Zhou, Tom Van Gerven, Muxing Guo, Allan Walton, Bart Blanpain

PII: S0925-8388(17)33075-X

DOI: 10.1016/j.jallcom.2017.09.046

Reference: JALCOM 43102

To appear in: *Journal of Alloys and Compounds*

Received Date: 16 April 2017

Revised Date: 4 September 2017

Accepted Date: 5 September 2017

Please cite this article as: M.A.R. Önal, C. Jönsson, W. Zhou, T. Van Gerven, M. Guo, A. Walton, B. Blanpain, Comparative oxidation behavior of Nd-Fe-B magnets for potential recycling methods: Effect of hydrogenation pre-treatment and magnet composition, *Journal of Alloys and Compounds* (2017), doi: 10.1016/j.jallcom.2017.09.046.

Comparative Oxidation Behavior of Nd-Fe-B Magnets for Potential Recycling Methods: Effect of Hydrogenation Pre-treatment and Magnet Composition

Mehmet Ali Recai Önal[¥*], Christian Jönsson[Φ], Wei Zhou[Φ], Tom Van Gerven[Ł], Muxing Guo[¥], Allan Walton[Φ], Bart Blanpain[¥]

[¥] High Temperature Processes and Industrial Ecology (HiTemp) Group, Department of Materials Engineering, KU Leuven, Kasteelpark Arenberg 44, 3001, Leuven, Belgium

[Φ] Magnetic Materials Group, School of Metallurgy and Materials, University of Birmingham, Edgbaston, Birmingham, B15 2TT, UK

[Ł] Process Engineering for Sustainable Systems (ProcESS), Department of Chemical Engineering, KU Leuven, Celestijnenlaan 200F, 3001 Leuven, Belgium

[*] Corresponding author. Tel.: +32 16 32 12 16; fax: +32 16 32 19 90.

E-mail address: mehmetalirecai.onal@kuleuven.be

Abstract

Recycling of Nd-Fe-B magnets is one of the few solutions to alleviate the supply risks of certain rare earth elements (REE) such as Nd and Dy. One of the most promising solutions with regards to extraction of end-of-life (EOL) magnets is to apply hydrogen decrepitation and to physically separate the Nd-Fe-B as a demagnetized hydrogenated powder. Such a powder can be directly recycled into new sintered magnets, or indirectly recycled by a conventional oxidation roasting and acid leaching flowsheet. The oxidation stability of powders, the microstructure after oxidation and the role of compositional variations can be of importance for the success of such subsequent direct or indirect recycling routes. In this study, magnets with varying compositions were subjected to different hydrogen treatments (e.g. hydrogenation, partial or full degassing and vacuum or conventional disproportionation) and subsequently studied for their comparative oxidation behavior and microstructural changes. While initial magnet composition was found to have little or no effect on oxidation behavior, the treatment type was found to have a direct impact on both the particle size distribution and the oxidation mechanism. The general oxidation rate was found to be the equally highest for hydrogenated and partially degassed samples followed by fully degassed and then disproportionated samples. After complete oxidation, complex REE-Fe-O compounds were formed more extensively in hydrogenated and fully degassed NdFeB samples than in the disproportionated samples.

Keywords: Recycling, Nd-Fe-B magnet, hydrogenation, decrepitation, disproportionation, oxidation.

1. Introduction

Nd-Fe-B magnets are the strongest magnets available, and they play an important role in the miniaturization of electronics, and in the transition to green energy systems [1]. Nd-Fe-B magnets are composed of around 30 % rare earth elements (REEs) (mainly Nd), around 70 % transition metals (mainly Fe) and ~1 % B [2]. Alterations to the composition may occur depending on the operational temperature and environment, availability and price of the constituents, and on the manufacturer. As for Dy, which is added for increased coercivity at elevated temperatures, the content can vary from close to 0 wt. % (hard disk drives, HDDs) to as high as 8.5 wt. % (electric car motors) [3]. Other REEs (Pr, Tb, Gd, Eu) or other elements such as Al, Co, Ga, Nb, Si and Zr can

also be present as minor admixtures to improve thermal or magnetic properties and oxidation-corrosion resistance of the magnets [4,5]. Due to the poor corrosion resistance, the magnets are often coated with Ni, Cu, Zn, Al, or epoxy.

In recent years, there have been instabilities in the supply chain of certain REEs, in particular Nd and Dy which are at the top of the critical materials list. Since the use of these elements is driven by the Nd-Fe-B market, recycling of such magnets has been identified as an important part of the solution to alleviate the supply risk [6].The recycling of end-of-life (EOL) magnets is today very limited due to serious barriers related to location and collection of Nd-Fe-B-containing waste streams, dismantling and extraction of the magnets, and finally the re-processing. Since the Nd-Fe-B is used in a wide range of applications, the methods cannot be standardized for all magnet-containing waste streams [7,8]. However a promising solution for extraction and re-processing of magnets from hard disk drives (HDDs) has been developed by the University of Birmingham. The damaged HDDs are loaded into a reactor, where hydrogen is introduced and selectively reacts with the Nd-Fe-B at room temperature, forming a demagnetized hydrogenated powder that is easily separated from the auxiliary materials [9]. This powder can then be directly recycled by milling, aligning, pressing, and re-sintering into new sintered magnets [10]. It was shown that addition of fresh Nd was required to compensate for the losses in magnetic properties due to oxidized portions of the magnet not liquefying during sintering [11–13]. Another direct recycling route is to apply the HDDR (Hydrogenation Disproportionation Desorption Recombination) process to produce a powder with refined grains for use in bonded magnets. This is done at high temperature in hydrogen where the $Nd_2Fe_{14}B$ matrix phase disproportionates into nano-scaled NdH_2 and Fe_2B in an α-Fe matrix, and recombines to sub-micron $Nd_2Fe_{14}B$ grains by the removal of the hydrogen atmosphere [14,15]. The hydrogenation-disproportionation treatment (without desorption and recombination steps) can also be used for production of microwave absorbing nanocomposite powders out of waste Nd-Fe-B magnets [16]. As an indirect recycling route, Fredericci et al (2014) studied both decrepitation and disproportionation methods followed by the addition of peroxide solution to produce Nd-oxide rich particles out of waste magnets [17].

However, the success of such direct or indirect recycling methods using hydrogenation treatments is very sensitive to the amount of oxidation and the compositional variations of the EOL magnets [15]. When the feed magnet is already heavily oxidized or the compositional variations are not acceptable, hydro- and/or pyrometallurgical flowsheets are required for recycling. One of the conventional methods is oxidative roasting and acid leaching which is a combination of pyro- and hydrometallurgical treatment [18–21]. Here, oxidative roasting is performed between 500-950 °C for up to 15 h depending on particle size and composition of the magnet and desired microstructure of the calcine. Due to oxidation, iron is in its ferric state, which on dissolution of the calcined material, precipitates at a pH around 3. This way it is possible to completely dissolve REEs into a leachate while leaving behind the major exogen (i.e. Fe) as useful solid hematite. However, only non-hydrogenated and as-recycled magnet materials were studied for their thermal oxidation and leaching behaviors up to now. From a different aspect, there are also studies regarding the oxidation-corrosion behavior of end magnet products [5,22–28]. Here, the main purpose is primarily to investigate the weakest spot of Nd-Fe-B magnets during their life cycle under oxidative and/or corrosive environments. Understanding of oxidation-corrosion mechanisms led to the use of coating materials and minor alloying additives including Ga, V, Nb, Co, Si etc. in the magnets to improve their resistance.

Although, the thermal and ambient oxidation behavior of non-hydrogenated magnet materials were broadly studied, there is limited information in open literature about oxidation behavior of hydrogenated magnets. Verdier et al. (1994) studied the ambient oxidation behavior of different master alloys for prolonged durations (up to 1200 h) after hydrogen decrepitation with or without partial or fully degassing [29]. Asada (1998) filed a patent where hydrogen gas was sent to the magnet scraps at 100-500 °C for pulverization purposes prior to oxidation roasting and acid leaching [30]. Although the hydrogenation treatment resembles the hydrogenation decrepitation process (except the application of heat), the composition and the initial state of the scrap (oxidized, corroded, etc.) are not known. Also, the information regarding the microstructural changes during hydrogenation and oxidation as well as the effects of hydrogenation pre-treatment or compositional variations in the magnet

scrap on the subsequent oxidation are not given. Instead, the leaching efficiencies of REE and Fe after different combinations of hydrogenation, oxidation and acid leaching conditions were reported in several examples.

Consequently, the thermal oxidation behavior of Nd-Fe-B with different hydrogen treatments requires a more comprehensive approach. Understanding of the oxidation stability of such hydrogen processed powders can be of importance for (i) the methodology and success of processes relying on hydrogenation treatments and (ii) adaptation of such methods as a pre-treatment (as in pulverization or microstructural modification) for subsequent conventional methods that rely on oxidation. As for example, if a hydrogen processed powder (e.g. hydrogenated, partially/fully degassed or disproportionated) is found to be highly stable even at high temperatures in open atmosphere, additional precautions, e.g. inert atmosphere, would be unnecessary during processing with treatments relying on hydrogenation. Otherwise, such precautions will be necessary to prevent the loss of hydrides via oxidation which has adverse effect on the downstream reprocessing routes. On the other hand, if a powder is found to be unstable in air, it could potentially be the best option for a process where oxidation is desired such as oxidative roasting. In this case, the microstructure of the calcine after a thermal oxidation treatment must be studied as it can be crucial for the subsequent methods such as in acid leaching. It was reported that when non-hydrogenated magnet materials are oxidized at high temperatures, complex $NdFeO_3$ is formed, which has higher acid resistance than the respective simple oxides [2]. Meanwhile, the effect of significant compositional variations in the magnets should also be studied while considering these possibilities. It is known that certain additives can result in different hydrogenation (i.e. Dy) and/or oxidation (i.e. Co, Cu, Al, etc.) behavior of the magnets [31,32]. As a consequence, in this study, 5 different hydrogenation treatments were applied to magnets with 3 different compositions. The produced samples were then comparatively oxidized while the calcines were characterized by several techniques in order to understand their oxidation nature. A similar methodology based on thermal oxidation treatment has been widely used in synthesis of thin cuprous oxide films for photovoltaic applications [33,34].

2. Materials and Methods

2.1. Materials Characterization

Chemical analysis of dissolved solid samples was performed with a Varian 720 ES model inductively coupled plasma optical emission spectrometer (ICP-OES). Small magnet pieces with known weights were dissolved in dilute HNO_3 acid solution and then diluted accordingly for measurements. The crystal structures of the hydrogenated and oxidized solid samples was characterized by a Bruker D2 PHASER X-ray diffractometer (XRD) with Cu-Kα X-ray radiation (30 kV;10 mA). The step size increment was 0.02 2-theta with 0.06 second/step. The raw data was processed both with the X'pert HighScore Plus PANalytical and Bruker-EVA software with ICDD database. Hydrogenated magnet samples were characterized using a JEOL 6060 model scanning electron microscope (SEM) and JEOL 7000 high resolution SEM (HR-SEM). Oxidized samples were also analysed using electron probe microanalysis (EPMA, JEOL JXA-8530F). Point analyses were taken with EPMA operated at 15 kV and $5x10^{-8}$ A. NdF_3, Fe_2O_3 and SiO_2 were defined as standards for Nd, Fe and O in analysis. Points that may appear relatively small in the figures were analysed at higher magnification. The thermal oxidation behaviour of hydrogenated magnet samples were comparatively analysed with T.A. Instruments Q600 model SDT (simultaneous differential scanning calorimetry (DSC) and thermogravimetric analysis (TGA)). 40-90 mg powder samples were heated from room temperature to 1000 °C at 10 °C/min under 100 mL/min dry air flow.

2.2 Sample Preparation

The uncoated sintered NdFeB magnet samples were supplied by Phillips, Southport (UK) (VCM composition) and Magneti Ljubljana - D.D. (Slovenia) (LG and HG compositions) in bulk form. The latter (LG and HG) were produced for the automotive industry, but failed visual standards and were rejected before magnetization as

secondary magnet materials. The samples were classified as voice coil magnet (VCM), low-grade (LG) and high-grade (HG) magnet samples in accordance with their application and Dy and Pr compositions, respectively. The samples of each composition were treated by 5 different hydrogenation methods, resulting in a total of 15 different sample types. All the samples were first hydrogen decrepitated (HD) according to the treatment procedure described in the following section. Some samples were degassed, to change the hydrogen content of the sample, either partially (PD) or fully (FD) at high temperatures under vacuum. Other samples were disproportionated, to change the microstructure, with two different methods: vacuum disproportionation (vHD) and conventional disproportionation (cHD), according to the methods described in the following section. After these hydrogenation treatments, the magnet batches were milled using a rotating blade mill and sieved below 250 µm. The sieved samples were then divided into ca. 1 g samples in glass vials. All these processes and transportation of the hydrogenated samples were performed under inert argon atmosphere in order to prevent any oxidation prior to the oxidation experiments. To determine the particle size distribution of powders, ca. 10 g of each sample type was dry screened with a series of sieves (63, 150 and 250 µm) on a shaker. Screened samples were then discarded due to the exposure to the atmosphere.

Hydrogenated and Degassed Samples (HD, PD and FD)

The bulk magnet samples were broken into pieces by a vice and loaded into a vacuum sintering furnace tube, which was flushed with argon and evacuated to 10^{-2} mbar. Subsequently, H_2 gas was introduced at constant 1200 mbar pressure at room temperature until the hydrogen decrepitation process was complete via Reaction (1) where x and y are ca. 1 and 1.25, respectively. The powder was then evacuated under inert atmosphere to prevent any oxidation. In order to partially desorb hydrogen from the HD sample via Reactions (2-3), it was heated to 500 °C under vacuum at a heating rate of 10 °C/min. The temperature was held constant at 300 and 500 °C for up to 2 h to allow time for the evacuation of the hydrogen from the system. To produce fully degassed samples and to remove the hydrogen that remained in the grain boundary phase (e.g. NdH_2), heating was continued to 900 °C. The powder was held at that temperature for 1 h in order to achieve complete desorption and evacuation of hydrogen via Reaction (4). Since FD samples had the same microstructure, the starting magnets were not studied in oxidation experiments.

$$Nd_2Fe_{14}B + Nd + (x + y)\ H_2 \rightarrow Nd_2Fe_{14}BH_{2x} + NdH_{2y} \quad (1)$$

$$Nd_2Fe_{14}BH_{2x} \rightarrow Nd_2Fe_{14}B + x\ H_2 \quad (2)$$

$$NdH_{2y} \rightarrow NdH_2 + (y\text{-}1)\ H_2 \quad (3)$$

$$NdH_2 \rightarrow Nd + H_2 \quad (4)$$

Hydrogen decrepitation (HD) followed by Disproportionation (vHD and cHD)

In order to produce vHD samples, the HD powder was heated at a rate of 15 °C/min under vacuum. The target temperature for the VCM composition was 900 °C. For LG and HG compositions it was 800 °C so as to ensure that disproportionation would occur below 1200 mbar H_2 pressure (maximum limit of the equipment). At the target temperature, hydrogen gas was introduced at a rate of 16 mbar/min up to the set pressure of 1200 mbar. These conditions were held for 1 h to ensure completion of disproportionation via Reaction (5). The furnace was then rolled off and the material was allowed to cool down under hydrogen atmosphere so as to prevent desorption and recombination of the hydrogenated powder with reversed Reaction (5). Then it was evacuated under inert atmosphere.

$$Nd_2Fe_{14}B + 2\ H_2 \rightarrow 2\ NdH_2 + 12\ Fe + Fe_2B \quad (5)$$

For the production of cHD samples, a similar route was followed as in the case for vHD samples. However, here the HD powder was heated under hydrogen atmosphere with 1200 mbar pressure to 950 °C at a heating rate of 15 °C/min and held for 5 hours to allow coarsening of the microstructure.

2.3. Furnace Experiments

After comparative non-isothermal thermogravimetric analyses (DSC-TGA) of 15 samples with 40-90 mg sample amount, non-isothermal furnace experiments were conducted in order to replicate the material at a larger scale and to produce a sufficient amount of oxidized samples for characterization analysis. For furnace experiments, a simple muffle furnace was used in open atmosphere. Selected magnet samples were weighed before each experiment and poured into a plate-like porcelain crucible. The initial room temperature of the muffle furnace was noted and heating to a predetermined final temperature was initiated. Once that temperature was reached the crucible was removed from the furnace and immediately flushed with nitrogen through a porous steel structure covering the surface of the hot crucible. This way further oxidation of the heated sample after the experiment was prevented while it cooled down to room temperature. The total duration of heating was also noted in order to calculate the average heating rate of the furnace. The sample weight was measured before and after the experiment in order to calculate weight (%).

3. Results and Discussion

3.1 Characterization of Materials

The chemical compositions of the starting magnet samples used in this study are given in Table 1. The high-grade sample (HG) contains high levels of Dy, Pr and Gd and a significant Al content. The low-grade sample (LG) contains a relatively high level of Dy but minor amounts of Pr and Gd along with a significant Co and Si presence as additives. The voice coil magnet (VCM) sample shows low levels of Dy, Pr and Gd as well as other additive elements. It should be noted that the Ni coating layer commonly found in VCM magnets was already peeled off after hydrogen decrepitation as it does not interact with the hydrogen gas. Due to its high ductility compared to the magnet powders, grinding operation to reduce the particle size did not affect these metal pieces as well. Then, it was possible to almost completely remove the Ni portions after subsequent sieving. Since all the sample preparation operations were conducted under oxygen-free environment, they did not affect the oxygen level in the samples.

Table 1 Composition of the magnets used in the study (wt. %).

Element	Nd	Pr	Dy	Gd	Fe	B	Al	Co	Cu	Ga	Nb	Si	Other	Total
HG	18.8	5.98	5.93	1.51	63.9	1.02	1.04	0.42	0.16	0.36	0.25	-	0.63	100
LG	26.1	0.68	2.68	0.02	63.5	0.73	0.35	2.99	0.12	0.54	-	1.49	0.80	100
VCM	25.7	3.43	1.32	-	66.7	1.00	0.31	1.30	0.10	0.05	-	0.02	0.10	100

Despite the compositional differences, the typical as-produced (non-hydrogenated) Nd-Fe-B phases are reported to be: the major matrix phase $Nd_2Fe_{14}B$, the minor phase $Nd_1Fe_4B_4$, and the Nd-rich grain boundary phase [35,36]. The XRD patterns of HG and LG after 5 hydrogenation treatments are given in Fig. 1 and they are comparable to each other as well to those obtained from VCM samples. During hydrogen decrepitation (HD), both the matrix and the grain boundary phases absorb hydrogen forming respective hydrides. The oxidized portion of the grain boundary phase does not react with hydrogen and remains in the oxide form. On partial degassing (PD), the matrix phase desorbs its hydrogen content completely while neodymium trihydride transforms to dihydride. When the powder is instead fully degassed (FD), the whole structure becomes hydrogen-free which is typical to that observed for any non-hydrogenated Nd-Fe-B magnets. In Fig. 2a, b and c, the backscattered SEM images of LG HD, PD and FD samples show similarities despite of differences in their hydrogen content. The bright spots are either one of the $NdH_{2.61}$ (HD)/NdH_2 (PD)/Nd (FD) or the oxidized and unreacted grain boundary phase. The dark regions are hydrogen containing (HD) or hydrogen free (PD and FD) matrix phase. Both HD and PD samples were found to contain many cracks and more fine particles than FD sample. When decrepitation was followed by disproportionation via Reaction (5), a different microstructure is obtained. For both vHD and cHD samples α-Fe, NdH_2/$NdH_{2.27}$ (or simply NdH_2) and Fe_2B are the constituting

phases along with few minor peaks that could not be identified with full confidence but are most likely oxide(s) of Nd which did not react during decrepitation and/or disproportionation (Fig. 1). Despite the same mineralogical appearances, the SEM images in Fig. 2d, e and f show differences between these samples. At low magnification, the vHD sample appears similar to HD, PD or FD samples but under HR SEM (Fig. 2f) it can be seen that NdH_2 phase is embedded lamellarly in the α-Fe matrix. Contrarily, due to coarsening by increased holding time under high pressure (1200 bar) and at high temperature (950 °C), these NdH_2 lamellas are replaced by homogenously distributed spheres in cHD sample that are visible even at low magnifications.

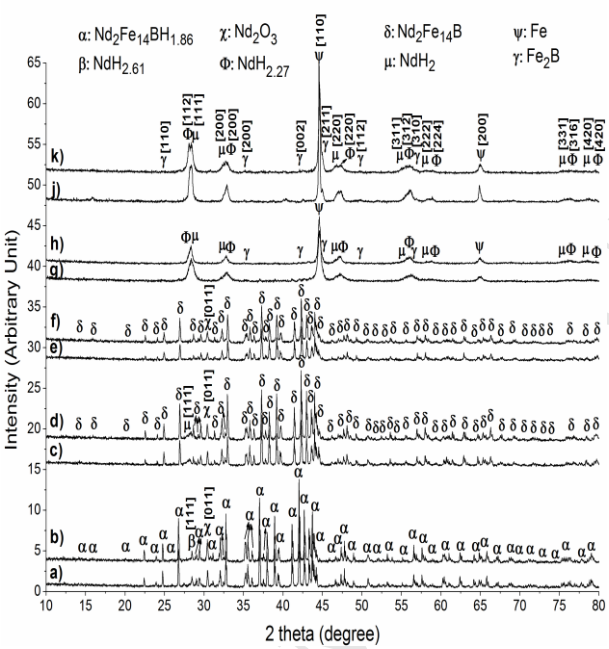

Fig. 1 XRD patterns of the HG (the lower patterns) and LG (the upper patterns) samples after (a-b) hydrogenation decrepitation (HD), (c-d) partial (PD) and (e-f) fully degassing (FD), (h-g) vacuum (vHD) and (k-j) conventional disproportionation (cHD).

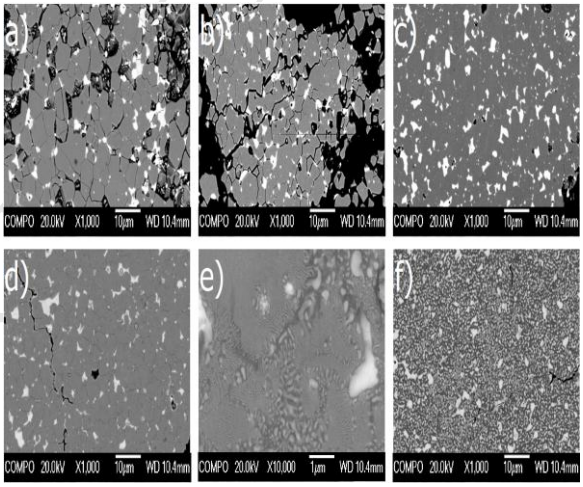

Fig. 2 SEM images of LG samples after (a) hydrogenation decrepitation (HD), (b) partial (PD) and (c) fully degassing (FD), (d-e) vacuum (vHD) and (f) conventional disproportionation (cHD).

Although all of the 15 samples were milled down to <250 µm, the friability of the material can be affected by the type of hydrogenation pre-treatment. This can vary the particle size distribution of the sample after milling and can therefore affect the subsequent oxidation kinetics. In Fig. 3, the particle size distributions of all samples are given within 3 different particle size classes. Also observed under SEM, a very high wt. % of particles of both HD and PD samples of all three compositions were quite fine despite minor variations between HG, LG or VCM. The fine particles form due to cracking along the grain boundary phase in the sintered magnets. For FD

samples of all three compositions, the particle size distribution is rather coarse compared to their HD or PD counterparts. The particles seem to be distributed more or less homogeneously among the size classes. That is caused by sintering of small particles during desorption of hydrogen at elevated temperatures (e.g. 900 °C) under vacuum. An identical situation to the FD samples is observed for cHD samples of all compositions. Only for the case of vHD samples, there seems to be an effect from compositional differences of the magnets. While LG and HG vHD samples are exceptionally coarse and fine, respectively, the VCM vHD sample assumes an FD/cHD-like distribution. In general, the friability of the magnet powder with respect to pre-treatment type can be summarized as: HD ≈ PD > HG vHD >> FD ≈ cHD ≈ VCM vHD > LG vHD.

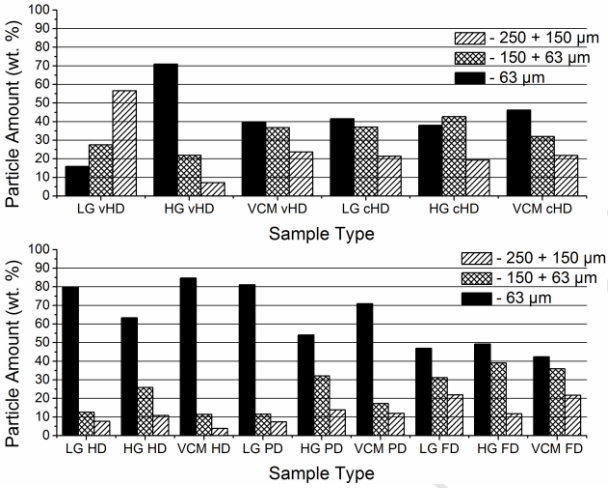

Fig. 3 Particle size distribution of all 15 samples.

3.2 Comparative Thermogravimetric Analysis (DSC-TGA Experiments)

Effect of Starting Composition

In Fig. 4, the non-isothermal oxidation weight (%) results of all 15 samples are shown. In hydrogenated, partially and fully degassed samples, the effect of composition on the weight (%) and therefore on the oxidation kinetics of the samples is negligible. Small and random variations are potentially caused by the minor differences in the particle size distribution. In vHD samples, the direct effect of varying particle size distribution is clearly visible throughout the heating: the finest HG sample is oxidized the fastest. Although all three compositions of cHD samples follow a similar weight (%) pattern, a sudden deviation occurs at ca. 750 °C. When Figs. 1 and 3 are considered, the effect of particle size distribution and the initial microstructure can be ruled out, as they are identical. Therefore, these deviations can only be correlated with the unique microstructure (e.g. spherical NdH_2 phase) obtained in cHD samples which seems to be sensitive to compositional variations: the high Co and Si contents in the LG sample delay its oxidation.

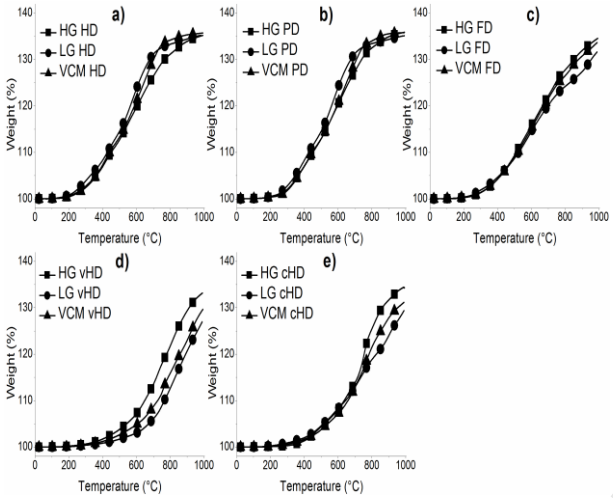

Fig. 4 Effect of starting composition on weight (%) of samples.

Fig. 5 shows the heat flow patterns that can be used for commenting on the nature of oxidation reactions of the samples. Once again these patterns are independent from composition for HD, PD and FD samples. While there are two exothermic reactions at ca. 400 and 600 °C for the first two, there is only one broad exothermic peak at ca. 500 °C for the latter. In HD and PD samples, this is likely to relate to the matrix phase and grain boundary phase oxidizing at different temperatures while in FD samples the oxidation seems to occur in a continuous manner. In vHD and cHD samples, it is hard to establish any correlation between the composition and the reaction temperatures due to the amount of noise in the traces. When Fig. 4 is considered, all these samples do not gain a significant weight (ca. <5 %) up to 600 °C. Hence, the majority of the oxidation reactions should be occurring at higher temperatures. These reactions can be grouped in two exothermic zones separated at ca. 750-800 °C.

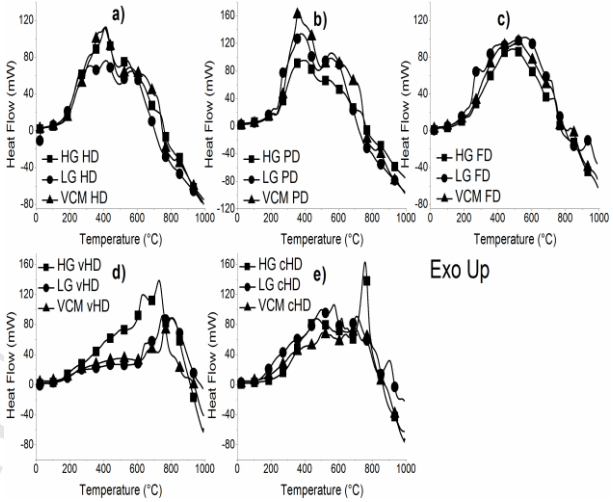

Fig. 5 Effect of starting composition on heat flow of the samples.

Effect of Hydrogenation Pre-treatment and Reproducibility of Results

In Fig. 6a, b and c, the weight (%) of the samples are given with respect to treatment type. All of the HD and PD samples reach the full oxidation state (i.e. a plateau in the figure) at temperatures lower than 900 °C while none of the FD or cHD samples reach full oxidation at temperatures below 1000 °C. Even with the exceptional particle fineness of the HG vHD sample (close to HG HD), none of the vHD samples reaches full oxidation either. In order to clear out any experimental errors (especially in the noisy vHD and cHD heat flow results), these DSC-TGA experiments were reproduced. In Fig. 6d, e and f, it can be seen that both weight (%) and heat flow results are quite identical. For all compositions, the general oxidation tendency increases as follows: HD ≈ PD > FD > cHD > vHD. This correlation is valid even when the other two parameters, starting composition and

particle size distribution, are the same or similar (e.g., HG HD and vHD samples). This is a clear indication that the microstructure after hydrogenation is an important parameter affecting the oxidation kinetics.

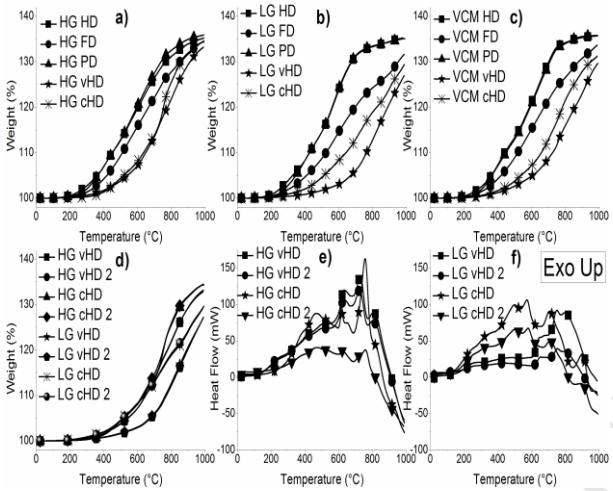

Fig. 6 (a-c) Effect of hydrogenation pre-treatment on oxidation behavior of the samples and (d-f) reproducibility of DSC-TGA experiments.

Although their hydrogen content varies, HD and PD samples share the similar microstructure as the non-hydrogenated sintered magnets (i.e. a Nd-rich grain boundary and a matrix phase). It has been shown earlier that the oxygen diffusion path in non-hydrogenated magnets occurs preferentially via the more reactive Nd-rich grain boundary phase, rather than via the $Nd_2Fe_{14}B$ matrix phase [5,24,26]. This phase is $NdH_{2.7}$ for HD and NdH_2 for PD samples. In vHD and cHD samples, there is no grain boundary phase after the disproportionation reaction but there is the α-Fe matrix with embedded lamellas or spheres of NdH_2 (Fig. 2). Hence, for these samples the oxygen diffusion path is the matrix itself. The ΔG^0 values for Reactions (6-8) at 500 °C are -3682 kJ, -3174 kJ and -859 kJ, respectively. In addition to their finer particle size distribution, HD/PD powders have slightly more reactive grain boundary phases than their FD counterparts allowing them to be oxidized faster. In vHD and cHD samples, however, the matrix phase (Fe) is quite stable compared to any Nd-containing grain boundary phase of the rest of the samples, leading to their comparatively slower oxidation kinetics.

$$2\ NdH_2 + 5/2\ O_2 \rightarrow Nd_2O_3 + 2\ H_2O \quad (6)$$

$$2\ Nd + 3/2\ O_2 \rightarrow Nd_2O_3 \quad (7)$$

$$3\ Fe + 2\ O_2 \rightarrow Fe_3O_4 \quad (8)$$

3.3 Furnace Experiments and Material Characterization

Based on the DSC-TGA results, it was decided to conduct the non-isothermal furnace experiments with final temperatures of 500 and 800 °C for HD, PD and FD samples. Only the LG composition was studied due to nearly identical behaviors of the other compositions in the previous experiments. For vHD and cHD samples, the final temperatures were 600, 750 and 900 °C. Both HG and LG compositions were studied for these samples due to dissimilar heat flow patterns obtained in Fig. 5d and e. All the experimental data obtained from furnace experiments are summarized in Table 2 together with those obtained from the DSC-TGA experiments. Differences between weight (%) values obtained from the furnace and DSC-TGA experiments are given in the last column of the same table.

Table 2 Comparative data between furnace (calculated heating rates are indicated) and DSC-TGA experiments (heating rate=10 °C/min).

Final Temperature	Sample Type	Average Furnace Heating Rate (°C/min)	Weight (%) (Furnace)	Weight (%) (DSC-TGA)	Weight (%) (Difference)
500	LG HD	12.6	114.7	114.6	0.19

	LG PD	12.5	114.5	114.6	-0.08
	LG FD	12.3	109.4	108.7	0.72
600	LG vHD	11.3	102.4	103.0	-0.62
	LG cHD	11.1	108.5	108.3	0.23
	HG vHD	11.4	107.2	107.2	-0.03
	HG cHD	11.3	107.9	108.1	-0.19
750	LG vHD	10.0	110.4	108.9	1.57
	LG cHD	10.2	118.0	116.0	2.06
	HG vHD	10.0	119.6	117.9	1.75
	HG cHD	10.1	123.2	119.4	3.72
800	LG HD	9.55	134.0	133.3	0.70
	LG PD	9.81	134.0	133.4	0.54
	LG FD	9.62	126.5	124.2	2.34
900	LG vHD	8.93	131.0	120.7	10.3
	LG cHD	9.01	132.1	124.0	8.09
	HG vHD	9.07	133.3	129.4	3.92
	HG cHD	8.93	134.7	131.7	2.97

For the samples with faster oxidation kinetics (e.g. HD and PD), the weight (%) results obtained in the furnace were in good agreement with those obtained in the DSC-TGA experiments. However, other samples with relatively slower kinetics (e.g. FD, vHD and cHD) generally showed higher weight (%) results in the furnace especially when the final temperatures were comparatively higher (e.g. 800-900 °C). That was because they were exposed to air for longer durations due to lower heating rates obtained in the furnace thereby increasing the reaction rates further.

Hydrogen Decrepitated and Degassed Magnets (HD, PD and FD)

In Fig. 7, the XRD patterns of LG HD, PD and FD samples obtained from heating to 500 and 800 °C are given. In all three patterns per final temperature, the phases are the same. While the temperature reaches to 500 °C, the hydrogen-free matrix phase in PD and FD samples dissociate via Reaction (9). Here, the $Nd_2Fe_{14}B$ phase dissociates to give initially amorphous Nd_2O_3 and Fe with minor B (or Fe_2B). In the case of HD samples, the hydrogen-containing matrix phase ($Nd_2Fe_{14}BH_2$) experience either a step-wise oxidation via first Reaction (10) then Reaction (9) or directly dissociates via Reaction (11) similar to Reaction (9). The point analysis results in Table 3 given for Fig. 8a and b indicate that the $Nd_2Fe_{14}BH_2$ (yellow zones) of the HD sample is already partially oxidized via one of these reaction paths.

$$Nd_2Fe_{14}B + 3/2\ O_2 \rightarrow Nd_2O_3 + 14\ Fe + B\ (PD\ and\ FD) \quad (9)$$

$$2\ Nd_2Fe_{14}BH_2 + O_2 \rightarrow 2\ Nd_2Fe_{14}B + 2\ H_2O\ (HD) \quad (10)$$

$$Nd_2Fe_{14}BH_2 + 2\ O_2 \rightarrow Nd_2O_3 + 14\ Fe + B + H_2O\ (HD) \quad (11)$$

After dissociation of the matrix phase, further oxidation involves only transformation of Fe to first magnetite (Reaction (12)) and then to hematite (Reaction (13)) as explained for the non-hydrogenated magnets [5,24,26]. The layer involving Fe and Fe_3O_4 is reported to be a thin transition zone between the outer non-protective hematite and inner fresh magnet layer [24]. That could be the reason why such transition regions are not clearly visible in the mapping result (Fig. 8b).

$$3\ Fe + 2\ O_2 \rightarrow Fe_3O_4 \quad (12)$$

$$4\ Fe_3O_4 + 2\ O_2 \rightarrow 6\ Fe_2O_3 \quad (13)$$

On the other hand, while hydrogen-containing grain boundary phases in HD and PD samples oxidize via Reactions (14-15), for hydrogen-free grain boundary phase in FD samples this proceeds via Reaction (7).

$$2\ NdH_3 + 3\ O_2 \rightarrow Nd_2O_3 + 3\ H_2O\ (HD) \quad (14)$$

$$4\ NdH_2 + 5\ O_2 \rightarrow 2\ Nd_2O_3 + 4\ H_2O\ (PD) \quad (15)$$

With further oxidation to 800 °C, the samples are completely oxidized (>30 % weight gain) and the well-established hematite and Nd-oxide peaks dominate the structure. Their interactions at high temperature for certain duration result in the formation of a REE-Fe complex oxide via Reaction (16). In Fig. 8c, 8d and in Table 3, it can be seen that the pink regions are Nd-oxide triple junctions while blue regions are hematite with finely dispersed small Nd_2O_3 crystals. The grey zones are representing the newly formed complex oxide grains. In acid leaching, it was reported that these complex oxides are more acid resistant than the respective simple oxides [19]. Since the complex oxide formation is quite abundant after oxidation of each sample type, a temperature lower than 800 °C should be preferred for higher REE leaching efficiencies. However, complete oxidation of especially Fe must also be satisfied in order to ensure Fe^{3+} precipitation at pH 2.5-3 and thus to obtain high REE purity in the leachate. This clearly also necessitates a temperature above 500 °C.

$$Nd_2O_3 + Fe_2O_3 \rightarrow 2\ NdFeO_3 \quad (16)$$

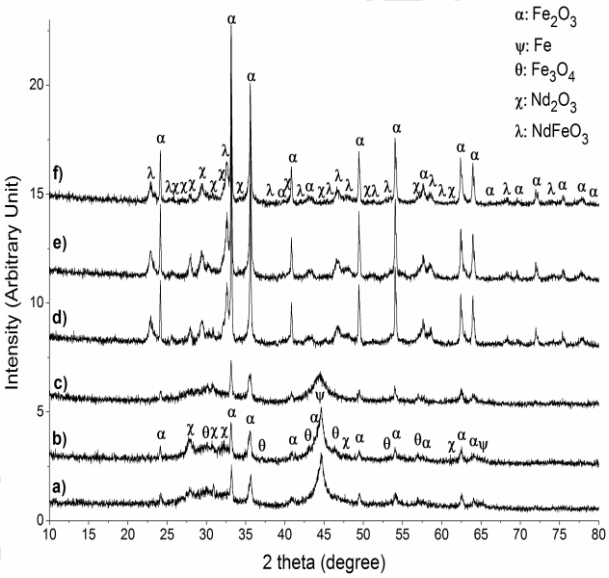

Fig. 7 XRD patterns of HD (the lower patterns), PD (the middle patterns) and FD (the upper patterns) of LG composition after non-isothermal oxidation in the furnace up to (a-c) 500 or (d-f) 800 °C, respectively.

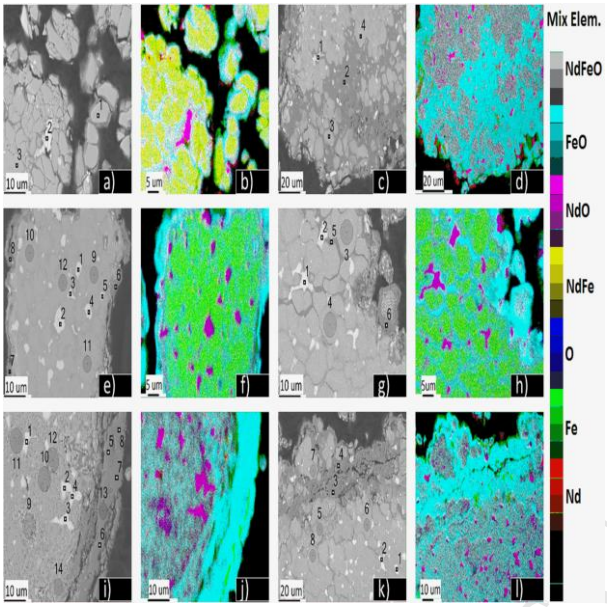

Fig. 8 Backscattered images and Nd-Fe-O mapping analysis of (a-b) LG HD 500 °C, (c-d) LG HD 800 °C, (e-f) HG vHD 750 °C, (g-h) HG cHD 750 °C, (i-j) HG vHD 900 °C and (k-l) HG cHD 900 °C (scale in color intensity).

Table 3 EPMA point analysis results of data points indicated in Fig. 8 (normalized to 100 wt. %).

Sample	Point No.	Al	O	Dy	B	Fe	Co	Nd
LG HD 500 °C	a-1	0.18	16.9	1.67	0.13	56.4	2.36	22.4
	a-2	0.01	26.4	1.91	0.00	6.38	0.72	64.6
	a-3	0.12	15.7	1.05	0.37	59.0	2.32	21.4
LG HD 800 °C	c-1	0.01	25.1	1.87	0.00	3.87	0.31	68.9
	c-2	0.03	35.1	0.00	0.00	61.7	1.82	1.44
	c-3	0.19	34.8	1.70	0.87	26.9	2.02	33.6
	c-4	0.17	30.6	1.74	0.65	28.5	5.26	33.0
HG vHD 750 °C	e-1-5	0.08	33.9	4.00	0.54	4.18	0.02	57.3
	e-6-8	0.09	30.2	0.04	0.00	64.7	0.12	4.85
	e-9-12	0.58	18.7	2.68	0.70	58.5	0.23	18.6
HG cHD 750 °C	g-1-2	0.04	31.8	6.39	0.00	3.61	0.53	57.6
	g-3-4	0.91	18.3	3.70	0.16	56.4	0.39	20.2
	g-5-6	0.08	30.4	0.30	0.04	63.0	0.04	6.19
HG vHD 900 °C	i-1-4	0.06	33.0	5.17	0.00	3.63	0.01	58.1
	i-5-8, 13	0.03	34.6	0.06	0.00	64.6	0.04	0.74
	i-9-12, 14	0.99	38.0	4.04	1.23	40.2	0.16	15.4
HG cHD 900 °C	k-1-2	0.00	30.7	5.90	0.00	2.12	0.00	61.3
	k-3-4	0.07	30.1	0.40	0.00	66.4	0.03	3.03
	k-5-8	0.97	37.5	3.14	0.00	39.5	0.18	18.6

Disproportionated Magnets (vHD and cHD)

Although DSC-TGA results proved that these two sample types are the most stable samples for all compositions and that they are therefore not good candidates for subsequent oxidative roasting and acid leaching, it is worthwhile to confirm the reason behind their higher oxidation resistivity (i.e. less reactive oxidation-diffusion medium in Reaction (8)) by studying their oxidation mechanism. In Figs. 9 and 10, the XRD patterns for cHD and vHD samples of both HG and LG compositions are given for the three studied final temperatures. After heating to 600 °C, both samples are barely oxidized with <10 % weight gain. Thus, the initial microstructures are mostly intact with only emerging peaks of iron and neodymium oxides. After heating to 750 °C, the differences between the samples become clearer. When the values in Table 2 are observed, HG and LG cHD samples with similar particle size distributions (Fig. 4) are oxidized quite similarly in the furnace as well but with higher levels than those in DSC-TGA. However, HG vHD sample is oxidized once again 10 % more than LG vHD due to the major difference in their particle size distributions (Fig. 4). After heating to 900 °C, contrary to the results in DSC-TGA, both HG and LG cHD samples reach (almost) full oxidation in the furnace. Despite the significant differences in their weight gain at lower temperatures (e.g. 600 and 750 °C), both vHD samples also reach (almost) full oxidation at 900 °C. These results show that the negative effects of additives and/or coarser particle size distribution can be overcome in a furnace although requiring prolonged heating at elevated temperatures with more contact area.

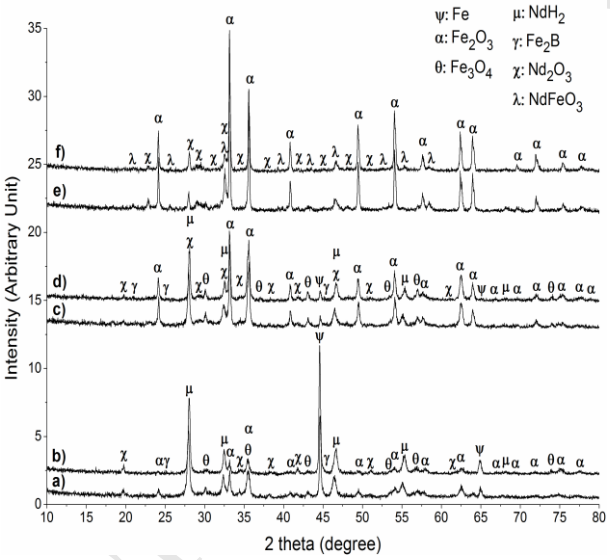

Fig. 9 XRD patterns of cHD samples of HG (the lower patterns) and LG (the upper patterns) compositions after non-isothermal heating to (a-b) 600, (c-d) 750 and (e-f) 900 °C, respectively.

Another important difference between cHD and vHD samples is the stability of NdH_2 phase. At 750 °C, most of this phase is still intact for cHD samples (peaks at ca. 55 2-theta, Fig. 9c and d), while it has mostly reacted to give Nd_2O_3 in vHD samples (Fig. 10c and d). This means that the coarsened spherical NdH_2 is more stable than the finer lamellar form. The oxidation-resistant minor additives such as Co can also contribute for that behavior which can also explain why compositional changes had a distinctive effect on oxidation of only cHD samples after 750 °C (Fig. 4). Here, these additives can accumulate preferentially in NdH_2 spheres thereby slowing their oxidation even further. A similar behavior may also cause such a deviation between the vHD samples (e.g. HG vHD is oxidized faster than LG vHD). However, the weight (%) patterns of all compositions start to deviate at very low temperatures due to dominant effect of particle size differences (Fig. 3). Hence, the effect of compositional variations in vHD samples, if there is any, is masked by that. As explained in section 3.2., the general oxidation tendency is higher for cHD samples than vHD samples. Therefore, more Fe must have been oxidized (and gained weight) in cHD samples to compensate for the lower weight gain by the slower oxidation of spherical NdH_2 compared to the lamellar form in the vHD samples. In other words, although lamellar NdH_2 is oxidized faster in vHD, it also somehow interferes with and delays the oxidation of the Fe matrix. This can also be observed when the intensities of Fe peaks at 45 2-theta value are compared between Figs. 9 and 10.

In Fig. 8g and h, it is clearly visible that hematite (blue) channels are formed in the HG cHD sample surrounding the clusters of fine (1-10 μm in diameter) NdH_2 spheres embedded in Fe (greenish-yellowish) that are only partially oxidized (Table 3). This preferred oxidation pattern is less visible for HG vHD in Fig.8e and 8f due to homogenous distribution of very fine (ca. 1 μm in width) NdH_2 lamellas within the Fe matrix. Because of this homogenous distribution and small sizes of lamellas and spheres, the grey zones in Fig. 8i-l representing coexistence of Nd-Fe-O can correspond either to a mixture of hematite and Nd_2O_3 crystals or to small $NdFeO_3$ crystals or to both. However, based on the XRD patterns in Figs. 9 and 10, the complex oxide formation is much less severe in disproportionated samples than in hydrogenated or degassed samples when they reach (almost) full oxidation. This means that not only the total weight gain but also the weight gain profile with respect to temperature is an important factor on the final microstructure. Reaction (16) necessitates the coexistence of primary oxides (e.g. hematite and Nd_2O_3) for a certain duration at elevated temperatures for the formation of such complex oxides. In HD/PD/FD samples, the existence of a reactive (Nd-rich) grain boundary phase already enables formation of some Nd-oxide crystals. More importantly, it also enables faster and homogenous dissociation of the matrix phase via Reactions (9-11) to subsequently form in-situ hematite and Nd-oxide. Contrarily, in vHD/cHD samples, oxidation has to proceed first through the more stable free iron matrix due to absence of a reactive Nd-rich grain boundary phase. In the meantime, the Nd-containing phases (i.e. lamellas or coarse spheres of NdH_2) in vHD/cHD samples are more isolated from the Fe-containing phases (i.e. free iron and Fe_2B) compared to the case in HD/PD/FD samples where the matrix phase (i.e. $Nd_2Fe_{14}B$ or $Nd_2Fe_{14}BH_{1.86}$) is the major source of both metals and thus their oxides. Hence, in addition to the total weight gain, the extent of complex oxide formation also depends on the oxidation of the whole structure without any delay in the formation of either primary oxide as well as their sufficient mixing and interaction at high temperatures. This factor is clearly dependent on the microstructure obtained by hydrogenation pre-treatment.

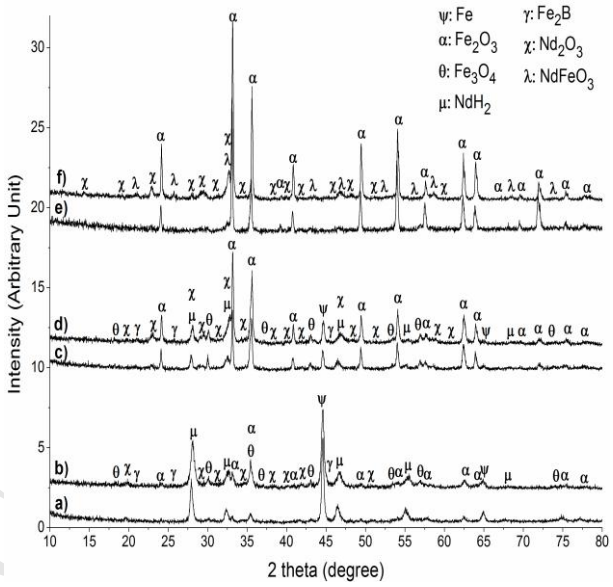

Fig. 10 XRD patterns of vHD samples of HG (the lower patterns) and LG (the upper patterns) compositions after non-isothermal heating to (a-b) 600, (c-d) 750 and (e-f) 900 °C, respectively.

4. Conclusions

In this study, it was aimed to comprehensively study several hydrogenation treatments and the thermal oxidation stabilities of the resulting Nd-Fe-B powders with three different compositions. The initial composition of the magnets was found to impose little or no effect on the oxidation behavior of both hydrogenated and as-produced/fully degassed magnets. Instead, the treatment type was found to impact directly on the oxidation kinetics of the powders via (i) particle size distribution (friability) and (ii) the oxidation-diffusion mechanism. The general correlation for particle fineness was found to be: HD ≈ PD > HG vHD >> FD ≈ cHD ≈ VCM vHD > LG vHD while for oxidation tendency it was: HD ≈ PD > FD > cHD > vHD or Hydrogenated > As-produced/Fully degassed > Disproportionated magnets. That was found to be mainly due to the reactivity order

of the oxidation diffusion/propagation medium as: NdH_3/NdH_2 (HD/PD) > Nd (FD) >> Fe (vHD/cHD). Consequently, for recycling routes where oxidation is required (e.g. oxidative roasting-acid leaching), hydrogen decrepitation treatment (HD) was found to be the best pre-treatment (which can also be used for physical extraction of Nd-Fe-B magnets from their surrounding). It was also found that the samples after disproportionation (without desorption and recombination) are highly stable and barely oxidized even when heated up to 600 °C in an open atmosphere. However, despite their faster oxidation kinetics, the formation of complex $NdFeO_3$ was found to be more extensive in HD/PD/FD samples than in vHD/cHD at (almost) full oxidation state. Hence, both the total weight gain and the weight gain profile with respect to temperature, which depends on the mineralogy after hydrogenation pre-treatment, are important factors for the extent of such complex oxide formation. As these oxides are reported to be problematic in subsequent acid leaching (i.e. more acid resistant), a close microstructural control may be required during roasting of the former powders. Alternatively, the intense complex oxide formation can be largely avoided by using vHD/cHD samples but with the cost of higher temperature roasting and thus higher energy consumption. Also, preparation of vHD/cHD samples are more complicated than that of HD/PD samples with once again higher temperature requirements as a consequence.

Acknowledgements

The research leading to these results has received funding from the European Community's Seventh Framework Programme ([FP7/2007-2013]) under grant agreement no. 607411 (MC-ITN EREAN: European Rare Earth Magnet Recycling Network). This publication reflects only the authors' view, exempting the Community from any liability. Project website: http://www.erean.eu. The authors gratefully acknowledge support from the Hercules Foundation (Project ZW09-09). Authors would like to thank Thu Hoai Le for her contribution to EPMA analysis and Joris Van Dyck for his contribution to furnace experiments.

References

[1] M. Sagawa, S. Hirosawa, H. Yamamoto, S. Fujimura, Y. Matsuura, Nd – Fe – B permanent magnet materials, Jpn. J. Appl. Phys. 26 (1987) 785–800.

[2] Y. Yang, A. Walton, R. Sheridan, K. Guth, R. Gauß, O. Gutfleisch, M. Buchert, B.-M. Steenari, T. Van Gerven, P.T. Jones, K. Binnemans, REE recovery from end-of-life NdFeB permanent magnet scrap : A critical review, J. Sustain. Metall. (2016). doi:10.1007/s40831-016-0090-4.

[3] K. Binnemans, P.T. Jones, B. Blanpain, T. Van Gerven, Y. Yang, A. Walton, M. Buchert, Recycling of rare earths: A critical review, J. Clean. Prod. 51 (2013) 1–22. doi:10.1016/j.jclepro.2012.12.037.

[4] J.M. Le Breton, J. Teillet, Mössbauer and X-ray study of NdFeB type permanent magnets oxidation: Effect of Al and Nb addition, J. Magn. Magn. Mater. 101 (1991) 347–348.

[5] I. Skulj, H.E. Evans, I.R. Harris, Oxidation of NdFeB-type magnets modified with additions of Co, Dy, Zr and V, J. Mater. Sci. 43 (2007) 1324–1333. doi:10.1007/s10853-007-2229-y.

[6] J. Kooroshy, G. Tiess, A. Tukker, A. Walton, Strengthening the european rare earths supply chain: Challenges and policy options. The European Rare Earths Competency Network (ERECON) Report, 2015.

[7] J.W. Darcy, H.M.D. Bandara, B. Mishra, B. Blanpain, D. Apelian, M.H. Emmert, Challenges in recycling end-of-life rare earth magnets, J. Miner. Met. Mater. Soc. 65 (2013) 1381–1382. doi:10.1007/s11837-013-0783-0.

[8] M. Panayotova, V. Panayotov, Review of methods for the rare earth metals recycling, Annu. Univ. Min. Geol. St. Ivan Rilski Part II, Min. Miner. Process. 55 (2012) 142–147.

[9] A. Walton, H. Yi, N.A. Rowson, J.D. Speight, V.S.J. Mann, R.S. Sheridan, A. Bradshaw, I.R. Harris, A.J. Williams, The use of hydrogen to separate and recycle neodymium-iron-boron-type magnets from electronic waste, J. Clean. Prod. 104 (2015) 236–241. doi:10.1016/j.jclepro.2015.05.033.

[10] I.R. Harris, A. Williams, A. Walton, J. Speight, Magnet recycling, US Patent Office. US2012/0137829A1, 2012.

[11] M. Zakotnik, I.R. Harris, A.J. Williams, Multiple recycling of NdFeB-type sintered magnets, J. Alloys Compd. 469 (2009) 314–321. doi:10.1016/j.jallcom.2008.01.114.

[12] M. Zakotnik, I.R. Harris, A.J. Williams, Possible methods of recycling NdFeB-type sintered magnets using the HD/degassing process, J. Alloys Compd. 450 (2008) 525–531.

doi:10.1016/j.jallcom.2007.01.134.
[13] M. Zakotnik, E. Devlin, I.R. Harris, A.J. Williams, Hydrogen decrepitation and recycling of NdFeB-type sintered magnets, in: Proc. 19th Int. Work. Rare Earth Perm. Magnets Their Appl., Central Iron and Steel Research Institute, 2006: pp. 289–295. doi:10.1016/S1006-706X(08)60197-1.
[14] Sheridan, R. S., Harris, I. R., A. Walton, The development of microstructure during hydrogenation–disproportionation–desorption– recombination treatment of sintered neodymium- iron-boron-type magnets, J. Magn. Magn. Mater. 401 (2016) 455–462.
[15] C. Jönsson, A. Zaim, W. Zhou, R.S. Sheridan, M.J.J. Degri, A. Bradshaw, The potential separation of neodymium from Nd-Fe-B magnets using the hydrogenation disproportionation reaction, in: O. Gutfleisch, M. Katter (Eds.), 24th Int. Work. Rare-Earth Futur. Perm. Magnets Their Appl. (REPM 16), Darmstadt, Germany, 2016: pp. 3–8.
[16] K. Miura, M. Masuda, M. Itoh, T. Horikawa, K. Machida, Microwave absorption properties of the nano-composite powders recovered from Nd–Fe–B bonded magnet scraps, J. Alloys Compd. 408–412 (2006) 1391–1395. doi:10.1016/j.jallcom.2005.04.025.
[17] C. Fredericci, M.F. De Campos, A.P.. . Braga, D.J. Nazarre, R. V. Martin, F.J.G. Landgraf, E.A. Périgo, Nd-enriched particles prepared from NdFeB magnets: A potential separation route, J. Alloys Compd. 615 (2014) 410–414. doi:10.1016/j.jallcom.2014.06.203.
[18] K. Koyama, M. Tanaka, The latest technology trend and resource strategy of rare earths, in: K. Machida (Ed.), CMC Press, Tokyo, 2011: pp. 127–131.
[19] J. Lee, W. Kim, J. Jeong, I.J. Yoon, Extraction of neodymium from Nd-Fe-B magnet scraps by sulfuric acid, J. Korean Inst. Metall. Mater. 36 (1998) 967–972.
[20] T. Vander Hoogerstraete, B. Blanpain, T. Van Gerven, K. Binnemans, From NdFeB magnets towards the rare-earth oxides: A recycling process consuming only oxalic acid, RSC Adv. (Accepted Manuscript). (2014). doi:10.1039/C4RA13787F.
[21] H.-S. Yoon, C.-J. Kim, J. Lee, S. Kim, J. Kim, J. Lee, Separation of neodymium from NdFeB permanent magnetic scrap, J. Korean Inst. Resour. Recycl. 12 (2003) 57–63.
[22] J.M. Le Breton, J. Teillet, Oxidation of (Nd,Dy)FeB permanent magnets investigated by 57Fe Mossbauer spectroscopy, IEEE Trans. Magn. 26 (1990) 2652–2654. doi:10.1109/20.104827.
[23] J. Jacobson, A. Kim, Oxidation behavior of NdFeB magnets, J. Appl. Phys. 61 (1987) 3763–3765.
[24] D.S. Edgley, J.M. Le Breton, S. Steyaert, F.M. Ahmed, I.R. Harris, J. Teillet, Characterisation of high temperature oxidation of Nd-Fe-B magnets, J. Magn. Magn. Mater. 173 (1997) 29–42. doi:http://dx.doi.org/10.1016/S0304-8853(97)00189-3.
[25] D.S. Edgley, J.M. Le Breton, D. Lemarchand, I.R. Harris, J. Teillet, Dissociation of Nd2Fe14B during high temperature oxidation, J. Magn. Magn. Mater. 128 (1993) L1–L7. doi:10.1016/0304-8853(93)90846-T.
[26] Y. Li, H.E. Evans, I.R. Harris, I.P. Jones, The oxidation of NdFeB magnets, Oxid. Met. 59 (2002) 167–182.
[27] S. Steyaert, J.M. Le Breton, J. Teillet, Kinetic parameters of the dissociation of Nd2Fe14B during oxidation determined by Mössbauer spectrometry, J. Phys. Condens. Matter. 10721 (1996) 10721–10736.
[28] I. Skulj, A.P. Douvalis, I.R. Harris, Characterisation of oxidation products of modified Nd-Fe-B type magnets, J. Alloys Compd. 407 (2006) 304–313. doi:10.1016/j.jallcom.2005.06.033.
[29] M. Verdier, J. Morros, D. Pere, N. Shell, I.R. Harris, Stability of Nd-Fe-B powders obtained by hydrogen decrepitation, IEEE Trans. Magn. 30 (1994) 657–659. doi:10.1109/20.312367.
[30] A. Asada, Method for recovering reusable rare earth compounds, US Patent Office. 5728355, 1998.
[31] R.S. Sheridan, A.J. Williams, I.R. Harris, A. Walton, Improved HDDR processing route for production of anisotropic powder from sintered NdFeB type magnets, J. Magn. Magn. Mater. 350 (2014) 114–118.
[32] K. Hirano, J. Kadono, S. Yamamoto, T. Tanabe, H. Miyake, Hydrogen-absorbing characteristics of 15 rare earth elements, J. Alloys Compd. 408–412 (2006) 351–354. doi:10.1016/j.jallcom.2005.04.052.
[33] Y. Abdu, A.. Musa, Copper (I) Oxide (Cu_2O) Based Solar Cells - A Review, Bayero J. Pure Appl. Sci. 2 (2009) 8–12.
[34] K.U. Isah, M.B. M, U. Ahmadu, U. Essang, M.I. Kimpa, J.A. Yabagi, Effect of oxidation temperature on the properties of copper oxide thin films prepared from thermally oxidised evaporated copper thin films, IOSR J. Appl. Phys. 3 (2013) 61–66.
[35] M.A.R. Önal, C.R. Borra, M. Guo, B. Blanpain, T. Van Gerven, Recycling of NdFeB magnets using sulfation, selective roasting, and water leaching, J. Sustain. Metall. 1 (2015) 199–215. doi:10.1007/s40831-015-0021-9.
[36] M.A.R. Önal, E. Aktan, C.R. Borra, B. Blanpain, T. Van Gerven, M. Guo, Recycling of NdFeB magnets using nitration, calcination and water leaching for REE recovery, Hydrometallurgy. 167 (2017) 115–123. doi:10.1016/j.hydromet.2016.11.006.

Highlights

- Thermal oxidation behaviors of NdFeB magnets are studied after 5 pre-treatments.
- Starting composition have negligible effect for hydrogenated and degassed magnets.
- Pre-treatment type impacts directly via friability and the oxidation-diffusion mechanism.
- General oxidation tendency is: hydrogenated > as-produced > disproportionated.
- Formation of complex $NdFeO_3$ was more extensive in HD/PD/FD samples than in vHD/cHD.